THE JOURNAL OF BIOLOGICAL CHEMISTRY VOL. 287, NO. 44, pp. 37330–37339, October 26, 2012

Palmitoylation-induced Aggregation of Cysteine-string Protein Mutants That Cause Neuronal Ceroid Lipofuscinosis*

Received for publication, June 14, 2012, and in revised form, August 9, 2012 Published, JBC Papers in Press, August 19, 2012, DOI 10.1074/jbc.M112.389098

Jennifer Greaves[‡], Kimon Lemonidis[‡], Oforiwa A. Gorleku[‡], Carlos Cruchaga[§], Christopher Grefen[¶], and Luke H. Chamberlain[‡1]

From the [‡]Strathclyde Institute of Pharmacy and Biomedical Sciences, University of Strathclyde, 161 Cathedral Street, Glasgow G4 0RE, Scotland, United Kingdom, the [§]Department of Psychiatry and Hope Center Program on Protein Aggregation and Neurodegeneration, Washington University, Saint Louis, Missouri 63130, and the [¶]Laboratory of Plant Physiology and Biophysics, Institute of Molecular, Cell, and Systems Biology, University of Glasgow, Glasgow G12 8QQ, Scotland, United Kingdom

Background: Specific mutations in the chaperone protein CSPα cause adult-onset neuronal ceroid lipofuscinosis.
Results: These mutants form SDS-resistant aggregates in a palmitoylation-dependent manner in cell lines and brain samples from mutation carriers.
Conclusion: Palmitoylation induces disease-causing CSPα mutants to form SDS-resistant aggregates.
Significance: Formation of SDS-resistant CSPα aggregates may underlie development of adult-onset neuronal ceroid lipofuscinosis.

Recently, mutations in the *DNAJC5* gene encoding cysteine-string protein α (CSPα) were identified to cause the neurodegenerative disorder adult-onset neuronal ceroid lipofuscinosis. The disease-causing mutations (L115R or ΔL116) occur within the cysteine-string domain, a region of the protein that is post-translationally modified by extensive palmitoylation. Here we demonstrate that L115R and ΔL116 mutant proteins are mistargeted in neuroendocrine cells and form SDS-resistant aggregates, concordant with the properties of other mutant proteins linked to neurodegenerative disorders. The mutant aggregates are membrane-associated and incorporate palmitate. Indeed, co-expression of palmitoyltransferase enzymes promoted the aggregation of the CSPα mutants, and chemical depalmitoylation solubilized the aggregates, demonstrating that aggregation is induced and maintained by palmitoylation. In agreement with these observations, SDS-resistant CSPα aggregates were present in brain samples from patients carrying the L115R mutation and were depleted by chemical depalmitoylation. In summary, this study identifies a novel interplay between genetic mutations and palmitoylation in driving aggregation of CSPα mutant proteins. We propose that this palmitoylation-induced aggregation of mutant CSPα proteins may underlie the development of adult-onset neuronal ceroid lipofuscinosis in affected families.

Neuronal ceroid lipofuscinoses (NCLs)[2] are a group of neurodegenerative disorders, with a hallmark accumulation of autofluorescent lipid- and protein-rich ceroid (lipofuscin) in neurons and other cell types (1). NCLs are classified as early infantile, late infantile, juvenile, and adult, depending upon the age of symptomatic onset. The genes affected in different NCLs have been characterized and encode predominantly lysosomal proteins (1); for example, mutations in the *CLN1* gene encoding the lysosomal enzyme protein palmitoyl thioesterase 1 can cause infantile NCL (2); protein palmitoyl thioesterase 1 functions in the removal of fatty acid groups from palmitoylated proteins during their lysosomal degradation (3).

Symptoms of adult-onset NCL (ANCL) usually precipitate before the age of 40 and lead to a significant decrease in life expectancy. Unlike other NCLs, which tend to be autosomal recessive, ANCL can be either autosomal recessive or autosomal dominant (4). Three studies published in 2011–2012 identified mutations in the *DNAJC5* gene encoding cysteine-string protein α (CSPα) as the cause of autosomal dominant ANCL in several unrelated families (5–7).

CSPα is a ubiquitously expressed DnaJ chaperone protein that regulates proteins involved in secretory vesicle dynamics (8–10). Knock-out of CSPα in mice leads to fulminant neurodegeneration (11), likely by destabilizing key synaptic proteins such as SNAP25 (12, 13) and dynamin (14, 15). The mutations in CSPα that cause ANCL occur within the highly conserved cysteine-string region, a heavily palmitoylated domain involved in membrane binding and intracellular targeting. The specific mutations identified were a substitution of leucine 115 by arginine (L115R) or a deletion of leucine 116 (ΔL116) (5–7).

The cysteine-string domain of CSPα plays a dual role in promoting stable membrane attachment (16, 17). First, the overall hydrophobicity of this region may allow transient membrane interaction of the nonpalmitoylated protein, allowing it to connect with membrane-bound Asp-His-His-Cys (DHHC) palmitoyltransferases. Subsequent palmitoylation of the cysteine-string domain by specific DHHC proteins promotes stable membrane attachment, facilitating trafficking to secretory vesicles and the plasma membrane. In addition, the cysteine-string

* This work was supported by Medical Research Council Senior Fellowship Award Grant G0601597 and Wellcome Trust Grant 094184 (to L. H. C.). This work was also supported by National Institutes of Health Grant P50 AG05681.
⌘ *Author's Choice*—Final version full access.
[1] To whom correspondence should be addressed. E-mail: luke.chamberlain@strath.ac.uk.
[2] The abbreviations used are: NCL, neuronal ceroid lipofuscinosis; ANCL, adult-onset NCL; CSPα, cysteine-string protein α; EGFP, enhanced GFP; SUS, split-ubiquitin system.

domain may also be involved in homodimerization and multimerization of CSPα (18).

The role of the cysteine-string domain in membrane binding, palmitoylation, and multimerization of CSPα suggests that ΔL116 and L115R mutations may perturb any one of these parameters. However, to date, analysis of the effects of the mutations have mainly used *in silico* modeling. A Kyte-Doolittle algorithm revealed a decrease in hydrophobicity of the cysteine-string domain for the L115R mutant and a smaller nonsignificant decrease for the ΔL116 mutant (6, 7). Additional *in silico* analysis revealed that both disease-causing mutations reduce the propensity of the cysteine-string domain to move from water to a phosphocholine bilayer interface, reducing the membrane affinity of CSPα (7). CSS-Palm software, which is used to identify putative palmitoylation sites, suggested a minimal effect of the mutations on palmitoylation *per se*, possibly with the modification of one cysteine compromised as a consequence of the L115R mutation (7). *In silico* analysis did not reveal a consistent effect of the mutations on protein aggregation; however, this analysis highlighted the high intrinsic tendency to form antiparallel β-sheets species of CSPα and the mutants (7). In addition to these *in silico* analyses, some experimental data were presented by Nosková *et al.* (6), which suggested that the mutants were mislocalized and exhibited a very modest decrease in palmitoylation.

Although potentially powerful, caution must be exercised when interpreting results of these *in silico* analyses for the following reasons: (i) the structure of the cysteine-string domain is not known, significantly weakening the reliability of nonexperimental measurements; (ii) aggregation propensity is not simply related to the amino acid sequence of CSPα but may also be dependent on the palmitoylation status of the protein and relative cytosol-membrane distribution; (iii) palmitoylation of CSPα is tightly linked with the intrinsic membrane affinity of the cysteine-string domain; (iv) palmitoylation prediction programs do not consider the properties of the individual DHHC proteins that modify CSPα. In short, the *in silico* analyses performed to date may not adequately (if at all) define how the L115R and ΔL116 mutations affect the cellular properties of CSPα and cause autosomal dominant ANCL.

EXPERIMENTAL PROCEDURES

Mammalian Plasmids and Mutagenesis—The human CSPα coding sequence lacking the initiating methionine and flanked by HindIII and BamHI restriction sites was synthesized by GeneArt (Invitrogen). Human CSPα contains an intrinsic HindIII restriction site, and this was removed by introducing a silent mutation (AAG→AAA). This CSPα sequence was inserted in-frame into the pEGFP-C2 vector. To generate myc-tagged constructs, bovine CSPα was excised from a myc-pcDNA3.1 construct (9) using BamHI and EcoRI enzymes and replaced with the human CSPα coding sequences. HA-tagged DHHC constructs were a kind gift from Masaki Fukata (19). The sequences of all plasmid constructs were verified by DNA sequencing (DNA Sequencing Service, Dundee, UK).

Antibodies—Rabbit polyclonal antibody recognizing CSPα was purchased from Stressgen (Victoria, Canada). HSC70 antibody was from New England Biolabs (Herts, UK). GFP antibody (JL8) was from Clontech. Rabbit Myc and mouse actin antibodies were from Abcam. Rat HA antibody (used for immunoblotting) was purchased from Roche Applied Science, and mouse HA antibody (used for immunofluorescence) was from Covance (Paris, France).

Cell Culture and Transfection—PC12 cells were cultured in RPMI 1640 medium with 10% horse serum and 5% fetal bovine serum. HEK293T cells were cultured in DMEM with 10% fetal bovine serum. All cells were grown in a humidified atmosphere at 37 °C and 5% (HEK293T) or 7.5% (PC12) CO_2.

Lipofectamine 2000 (Invitrogen) was used for all transfections at 2 μl/μg DNA. For confocal microscopy, PC12 cells were plated on poly-D-lysine glass coverslips and transfected with 0.5 μg of EGFP-CSPα plasmids and analyzed ~40 h later. For biochemical analysis, PC12 cells growing on poly-D-lysine-coated 24-well plates were transfected with 1 μg of plasmid DNA and analyzed ~40 h after transfection. HEK293T cells were transfected with 0.8 μg of EGFP-CSP and 1.6 μg of the indicated HA-tagged DHHC constructs and analyzed ~20 h later.

Cell Fixation, Labeling, and Confocal Microscopy—Transfected cells were fixed in 4% formaldehyde. For antibody staining, the cells were then permeabilized in 0.25% Triton X-100 (in PBS with 0.3% BSA) and incubated successively with primary antibody (1:50) and Alexa Fluor 546-conjugated secondary antibody (1:400; Invitrogen). The cells were then washed in PBS, air-dried, and mounted on glass slides in Mowiol. A Leica SP5 laser scanning confocal microscope was used to view cellular fluorescence. Image stacks of PC12 cells were acquired at Nyquist sampling rates and deconvolved using Huygens software (Scientific Volume Imaging).

SDS-PAGE—Samples were diluted in SDS-dissociation buffer (final concentration 2% SDS, 25 mM DTT, 10% glycerol, 0.01% bromphenol blue, 50 mM Tris, pH 6.8) heated to 100 °C for 5 min and loaded onto 12% polyacrylamide gels.

Cell Fractionation—Transfected PC12 or HEK293T cells on 24-well plates were resuspended in a buffer containing 5 mM Hepes, and 1 mM EDTA, pH 7.4, supplemented with a protease inhibitor mixture (Sigma) and with or without 1% Triton X-100. The cells were frozen at −80 °C, thawed, and centrifuged at 16,000 × *g* for 30 min at 4 °C. Recovered supernatant and pellet fractions were made up to an equal volume in SDS-dissociation buffer and resolved by SDS-PAGE.

Preparation of Human Brain Lysates—Lysates from human postmortem brain samples were prepared by homogenization (Dounce homogenizer) in ice-cold buffer composed of 20 mM Hepes, 250 mM sucrose, 1 mM $MgCl_2$, 2 mM EDTA, 1% Triton X-100, and protease inhibitor mixture (Sigma), pH 7.4. Insoluble material was removed by centrifugation 4000 × *g* for 10 min. Cortical brain tissue from histologically characterized normal brain tissues authorized for ethically approved scientific research (Lothian Research Ethical Committee; reference 2003/8/37) were gratefully provided by Robert Walker at the Medical Research Council Sudden Death Brain and Tissue Bank, University of Edinburgh (20). Cortical tissue from ANCL patients carrying the L115R mutation was obtained from Washington University School of Medicine in St. Louis ADRC. All tissue used was from anonymized patients, and ethical

approval for the work was granted by the University of Strathclyde (reference UEC1112/46).

Chemical Depalmitoylation of CSPα—Human brain lysates (100 μg of protein) were incubated overnight at room temperature in 0.5 M hydroxylamine, pH 7, or 0.5 M Tris, pH 7, supplemented with a protease inhibitor mixture (Sigma). EGFP-CSPα exhibited proteolysis following extended incubation times in hydroxylamine, and therefore cells expressing EGFP-tagged constructs were treated with 0.5 M Tris-HA for 2 h. Following treatment, the cell samples were diluted in SDS-dissociation buffer and resolved by SDS-PAGE.

[^{3}H]Palmitic Acid Labeling Experiments—Transfected HEK293T cells were washed in DMEM supplemented with 10 mg/ml defatted BSA and then incubated in the same medium containing 0.5 mCi/ml [^{3}H]palmitic acid (PerkinElmer Life Sciences) for 3 h. Cells were then lysed in SDS-dissociation buffer, resolved by SDS-PAGE, and transferred to nitrocellulose. Duplicate nitrocellulose membranes with either processed for immunoblotting or used for detection of ^{3}H signal with the aid of a Kodak Biomax Transcreen LE intensifier (PerkinElmer Life Sciences).

Split Ubiquitin System—Gateway-compatible mouse DHHC17/DHHC3 and human CSPα cDNAs were produced by PCR and inserted using Gateway technology into pDONR207 and then into pMetYC-Dest (bait plasmid) and pNX32-Dest (prey plasmid) respectively. After transformation of THY.AP4 and THY.AP5 yeast strains with bait and prey plasmids, respectively, the two strains were mated. Growth of diploid cells was monitored after dropping of 5 μl of each yeast suspension (at A_{600} 1 or 0.1) on synthetic defined medium plates (1.7 g/liter yeast nitrogen base without ammonium sulfate, 5 g/liter ammonium sulfate, 20 g/liter glucose, 1.5 g/liter CSM-Ade,-His,-Trp,-Leu,-Ura,-Met drop-out mix, and 20 g/liter agar) and subsequent growth for 4 days at 30 °C (for interactions with DHHC17) or 7 days (for interactions with DHHC3). As a loading control and to verify matings, the same amounts were dropped onto plates with synthetic defined medium supplemented with adenine and histidine, and growth was monitored after 3 days at room temperature. Yeast transformations, mating, and sample preparation for Western blotting were performed as described in Ref. 21.

Quantification and Statistical Analyses—Densitometric quantification of immunoblots was performed using ImageJ software (National Institutes of Health). Statistical analyses was by a one-way ANOVA using the Analyze-It plugin for Microsoft Excel; a p value of <0.05 was taken to represent statistical significance. For quantification of aggregation, the density of aggregates was expressed as a ratio to monomeric forms of the protein (corresponding to the sum of the nonpalmitoylated and palmitoylated bands).

RESULTS

Mutant CSPα Proteins Are Mistargeted and Form SDS-resistant Aggregates—A schematic diagram of the domain structure of CSPα is shown in Fig. 1*A*, highlighting the position of the residues (leucine 115 and leucine 116) that are mutated in ANCL. As a first step toward the identification of acquired biochemical properties of CSPα proteins containing the ΔL116 and L115R mutations, EGFP-tagged forms of these proteins were expressed in neuroendocrine PC12 cells and analyzed by confocal microscopy and SDS-PAGE/immunoblotting. Wild-type EGFP-CSPα associates with the plasma membrane and vesicles in PC12 cells (16) (Fig. 1*B*, *left*). In contrast, both the ΔL116 and L115R mutants displayed a more dispersed and punctate localization and a reduced plasma membrane staining (Fig. 1*B*, *middle* and *right*).

As intracellular targeting of CSPα is dependent upon multiple palmitoylation of the cysteine-string domain (16), we next examined whether this modification was perturbed for the mutant proteins. The palmitoylation status of CSPα can be readily assessed by its migration profile on SDS gels, as the fully palmitoylated form of the protein migrates approximately 7 kDa heavier than the nonpalmitoylated protein (16, 17, 22). The migration of palmitoylated (*p*) and nonpalmitoylated (*np*) bands of wild-type EGFP-CSPα expressed in PC12 cells is shown in Fig. 1*C* (note that we confirm that the upper band is palmitoylated in subsequent figures). Interestingly, for the ΔL116 and L115R mutants there was a clear absence of palmitoylated monomeric forms of the proteins (Fig. 1*C*), and the mutations induced the formation of SDS-resistant aggregates (Fig. 1*C*, quantified in the *right panel*). These aggregates migrated predominantly as two distinct higher molecular mass bands, with the upper band remaining in the stacking gel (Fig. 1*C*). To confirm that aggregation was not dependent on the EGFP tag, myc-tagged forms of the CSPα proteins were also examined, confirming the near absence of palmitoylated monomeric forms of the mutant proteins and formation of high molecular mass aggregates (Fig. 1*D*).

In contrast to the L115R mutant, a CSPα(L115A) mutant exhibited the same migration profile on SDS gels as wild-type CSPα (Fig. 1*E*), demonstrating that the defects in the L115R and ΔL116 mutants likely arise due to a loss of overall hydrophobicity rather than a specific requirement for an intact dileucine motif.

Finally, we examined whether the mutant aggregates were cytosolic or membrane-associated. For this, transfected PC12 cells were disrupted by freeze/thawing and fractionated into cytosol and membrane fractions by centrifugation. Immunoblotting for glyceraldehyde-3-phosphate dehydrogenase (GAPDH) and syntaxin 1A confirmed the successful separation of cytosolic and membrane proteins in supernatant and pellet fractions, respectively (Fig. 1*F*). The ΔL116 and L115R aggregates were enriched in the membrane fraction (Fig. 1*F*). To confirm that the aggregates are truly membrane-associated and not pelleting due to their large size, the fractionation protocol was also performed in the presence of Triton X-100 to solubilize bulk cellular membranes. Under these conditions, the majority of the mutant aggregates did not pellet, supporting the idea that they are predominantly membrane-associated in PC12 cells.

CSPα Mutants Display Efficient Interaction with DHHC Palmitoyltransferases—The cysteine-string domain of CSPα, where the disease-causing mutations occur, has 14 cysteine residues in a span of 24 amino acids. One possibility to explain the observed aggregation of CSPα mutants is that the mutations prevent palmitoylation of the protein, and aggregation is caused

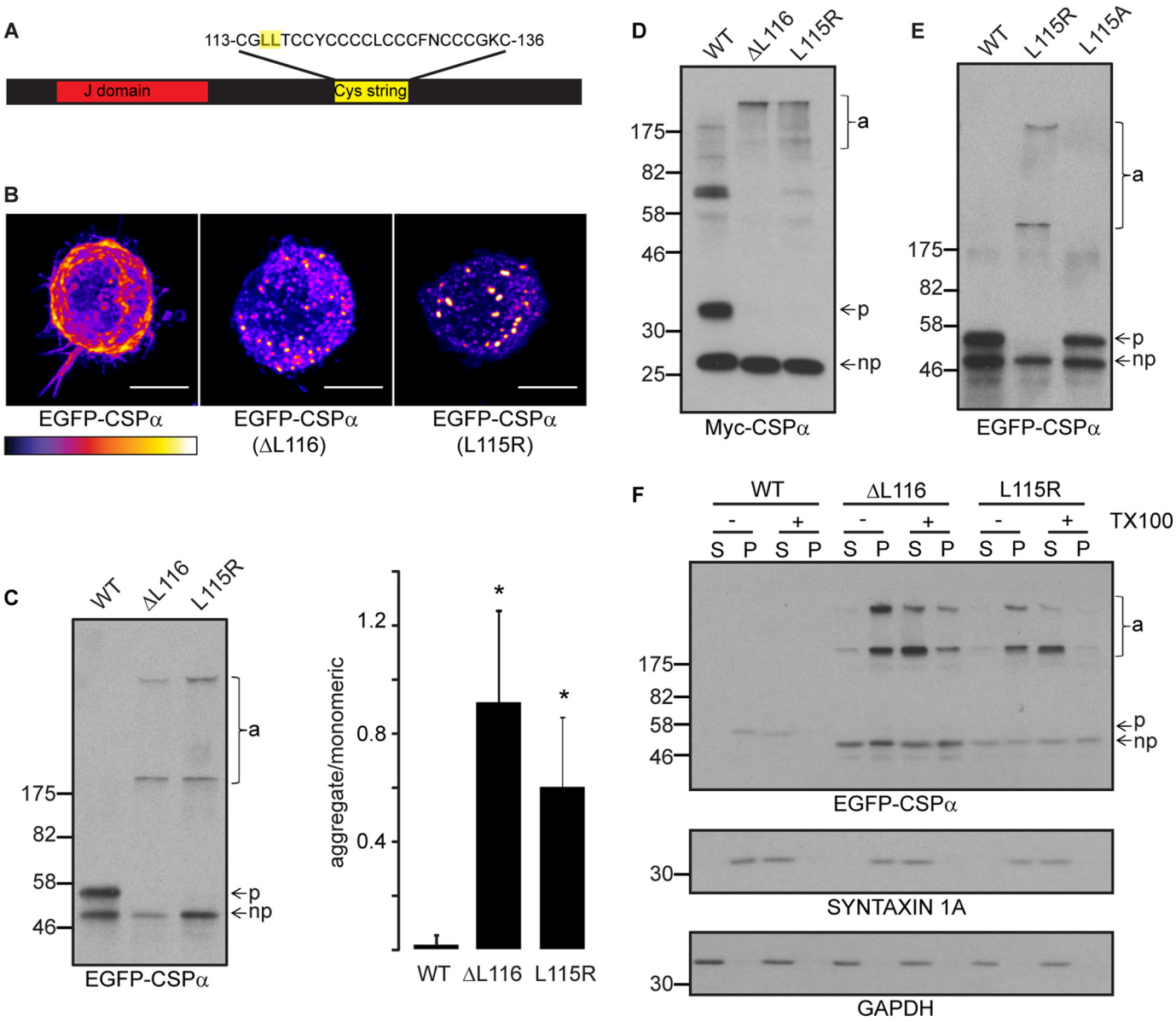

FIGURE 1. **Localization and biochemical properties of L115R and ΔL116 mutants in PC12 cells.** *A*, schematic diagram of CSPα showing relative positions of the DnaJ and cysteine-string domains and highlighting the positions of amino acids lysine 115 and 116. *B*, PC12 cells transfected with EGFP-tagged CSPα constructs and examined by confocal microscopy. Representative maximum intensity projections of deconvolved image stacks are presented for the localization of each construct. *Scale bars* represent 5 μm, and the color coding of fluorescence intensity profile is indicated. *C*, *left panel*, migration profile of wild-type and mutant forms of EGFP-tagged CSPα proteins on SDS gels revealed by immunoblotting with anti-GFP. *Right panel*, mean values ± S.E. (*error bars*) for the ratio of aggregated to monomeric forms of the proteins ($n = 4$). The data were analyzed using a one-way ANOVA, *asterisks* denote a significant difference from wild-type CSPα ($p < 0.05$). *D*, migration profile of wild-type and mutant forms of myc-tagged CSPα on SDS gels revealed by immunoblotting with anti-myc antibody. *E*, migration profile of wild-type and mutant forms of the indicated EGFP-tagged CSPα constructs on SDS gels revealed by immunoblotting with anti-GFP antibody. *F*, PC12 cells expressing the indicated CSPα proteins separated into supernatant (*S*) and pellet (*P*) fractions, containing cytosolic and membrane proteins, respectively. The fractionation was performed in the presence and absence of 1% Triton X-100 as indicated. Equal volumes of the recovered samples were resolved by SDS-PAGE, transferred to nitrocellulose, and probed with antibodies against GFP, syntaxin 1A, and GAPDH. *C–F*, *a* denotes aggregates, *p* shows position of palmitoylated monomeric CSPα, and *np* highlights the nonpalmitoylated monomers. Positions of molecular mass markers are shown on the *left*.

by the presence of many unmodified cysteines. To examine this, we first tested whether the mutations blocked interaction with DHHC palmitoyltransferases. In mammalian cells at least 24 DHHC proteins are expressed (23), and CSPα can be palmitoylated by DHHC3, DHHC7, DHHC15, or DHHC17 (17). Here, we focused on the interaction of CSPα with DHHC17 and DHHC3; knock-out of DHHC17 led to a complete loss of CSP palmitoylation in *Drosophila* (24). The split-ubiquitin system (SUS) was used to study the interaction between CSPα proteins and DHHC17/3 (21). This assay depends on the release of LexA-VP16 transactivator following reassembly of N- and C-terminal halves of ubiquitin, which are fused to the interacting proteins of interest. Reassembled ubiquitin is cleaved by ubiquitin-specific proteases, leading to the release of LexA-VP16. Nuclear translocation of LexA-VP16 allows yeast cells to grow on media lacking adenine and histidine. No major difference was detected in the ability of wild-type CSPα or the ΔL116 and L115R mutants to interact with DHHC17 in the SUS (Fig.

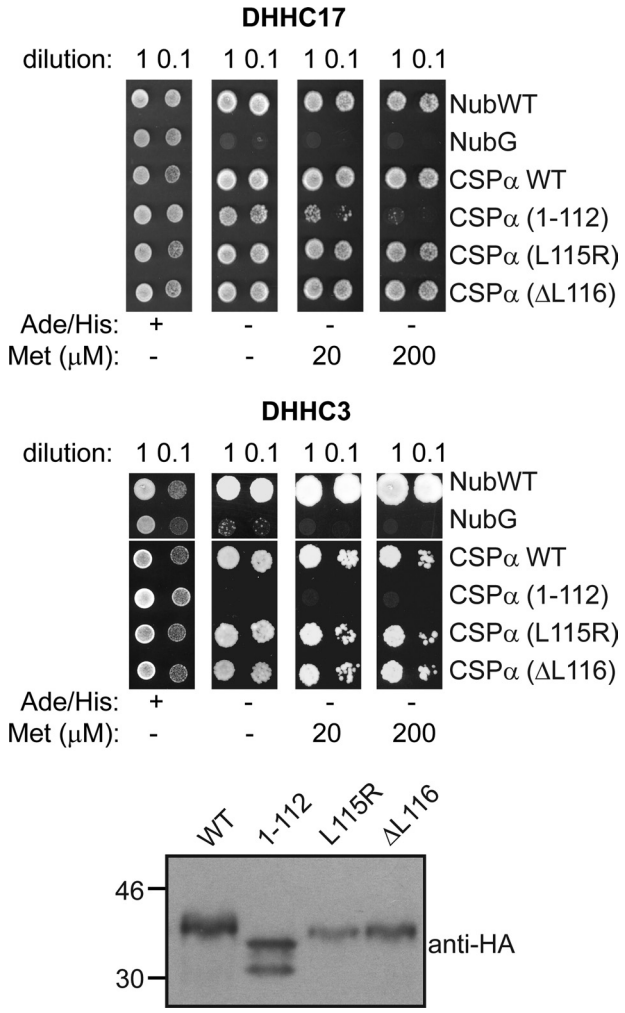

FIGURE 2. **Interaction of CSPα mutants with DHHC palmitoyltransferases.** Yeast diploids were created by mating cells expressing a C-terminal half of ubiquitin and PLV (protein A-LexA-VP16) tag fused to the C termini of DHHC17 (*top panel*) or DHHC3 (*middle panel*) with cells expressing the wild-type form of the N-terminal half of ubiquitin (*NubWT*; positive control), a mutant form of the N terminus that does not spontaneously reassemble with the C terminus of ubiquitin (*NubG*; negative control), or NubG fused to the N terminus of wild-type CSPα, or L115R, ΔL116, and CSPα(1–112) mutants. Diploids were spotted onto medium containing adenine (*Ade*) and histidine (*His*) to verify equal plating density and plated on medium lacking Ade/His to determine protein-protein interaction; methionine was added to confirm interaction at lower expression levels. *0.1* and *1* refer to the A_{600} of liquid culture dropped onto the plates. Yeast diploids containing DHHC17 and all CSPα constructs displayed growth on plates without Ade/His (*second panel*); however, under more stringent conditions in the presence of methionine (expression of the bait is regulated by a methionine-repressible promoter) (*third* and *fourth panels*) growth of cells expressing the 1–112 mutant was lost, whereas wild-type, L115R, and ΔL116 constructs all supported growth. Similar results were obtained with DHHC3, although in this case no growth was detected in diploids containing DHHC3 and the 1–112 mutant on any plates lacking Ade/His. Images for growth on plates lacking Ade/His were taken after 4 days for DHHC17 and 7 days for DHHC3. The *bottom panel* shows an immunoblot probed with anti-HA, confirming expression of all of the CSPα constructs; positions of molecular mass markers are shown on the *left*.

2). In contrast, a CSPα mutant truncated before the cysteine-string domain (amino acids 1–112) displayed a greatly reduced interaction with DHHC17 under stringent conditions (with 200 μM methionine), confirming the ability of the system to report reliably on protein-protein interactions. The interaction of CSPα with DHHC3 in the SUS was weaker than with DHHC17. Nevertheless, longer growth times (7 days compared with 4 days for DHHC17) allowed a robust measurement of CSPα-DHHC3 interaction. As with DHHC17, no difference was detected in the ability of wild-type and mutant CSPα proteins to interact with DHHC3; no interaction was detected between DHHC3 and CSPα(1–112) under any conditions.

Co-expression of Active DHHC Proteins Promotes Aggregation of CSPα Mutants—The results of the SUS (Fig. 2) did not uncover a difference in the interactions of the mutant CSPα proteins with DHHC3 and DHHC17. To investigate palmitoylation of the CSPα mutants further, we co-expressed these proteins with DHHC3 in HEK293T cells. In contrast with PC12 cells (Fig. 1), overexpressed wild-type CSPα is only weakly palmitoylated in HEK293T cells, but co-expression of specific DHHC proteins (including DHHC3) leads to a large increase in palmitoylation of CSPα (17). As described previously (17), co-expression of DHHC3 increased palmitoylation of wild-type CSPα, as detected by a shift in migration on SDS gels (Fig. 3*A*). Interestingly, the CSPα mutants exhibited a low level of aggregation in HEK293T cells when expressed individually, and this aggregation was markedly increased by co-expression of DHHC3 (Fig. 3*A*). Note that DHHC3 did not co-aggregate with the mutant CSPα proteins (Fig. 3*A*, *lower*). In addition to promoting aggregation of the CSPα mutants, co-expression with DHHC3 also led to redistribution of the ΔL116 and L115R proteins from the cytosol onto Golgi membranes (Fig. 3, *B* and *C*). Note that CSPα is not efficiently trafficked onto post-Golgi membranes in this co-expression assay in HEK293T cells, explaining the difference in localization with PC12 cells (Fig. 1*B*). We also confirmed that the mutant aggregates were membrane-associated following DHHC3 co-expression by cellular fractionation (Fig. 3*D*).

Before proceeding with further analyses of CSPα palmitoylation and aggregation, we examined whether the conditions used in sample preparation for SDS-PAGE (including heating samples to 100 °C in 25 mM DTT) might be affecting palmitoylation or aggregation of the mutant CSPα proteins. For this, we compared the migration of wild-type and mutant CSPα proteins on SDS gels following preparation in SDS sample buffer containing 1, 5, and 25 mM DTT and with or without sample boiling. Fig. 3*E* shows that there was very little difference in the migration of mutant CSPα proteins under the different conditions tested except for the appearance of a small amount of a band corresponding in size to dimeric CSPα (band slightly below the 175-kDa molecular mass marker) in nonboiled samples, the presence of which was more pronounced with the wild-type protein.

Having confirmed that palmitoylation and aggregation of the mutant CSPα proteins was not being significantly affected by the sample preparation conditions, we proceeded to examine the effects of DHHC proteins on mutant CSPα aggregation further. We examined whether the increase in aggregation of mutant CSPα proteins occurred with other DHHC proteins and whether it required the palmitoyltransferase activity of these proteins (palmitoyltransferase activity is abolished by mutation of the DHHC motif to DHHS). Indeed, aggregation of the CSPα mutants was promoted by co-expression with DHHC3, DHHC7, and DHHC17 but not by the inactive forms of these palmitoyltransferases (Fig. 3*F*). These findings clearly

link palmitoylation by DHHC proteins with the induction of aggregation of CSPα proteins carrying the L115R or ΔL116 mutations.

CSPα Mutant Aggregates Are Disrupted by Chemical Depalmitoylation—Only active forms of DHHC 3/7/17 are able to promote aggregation of the CSPα ΔL116 and L115R

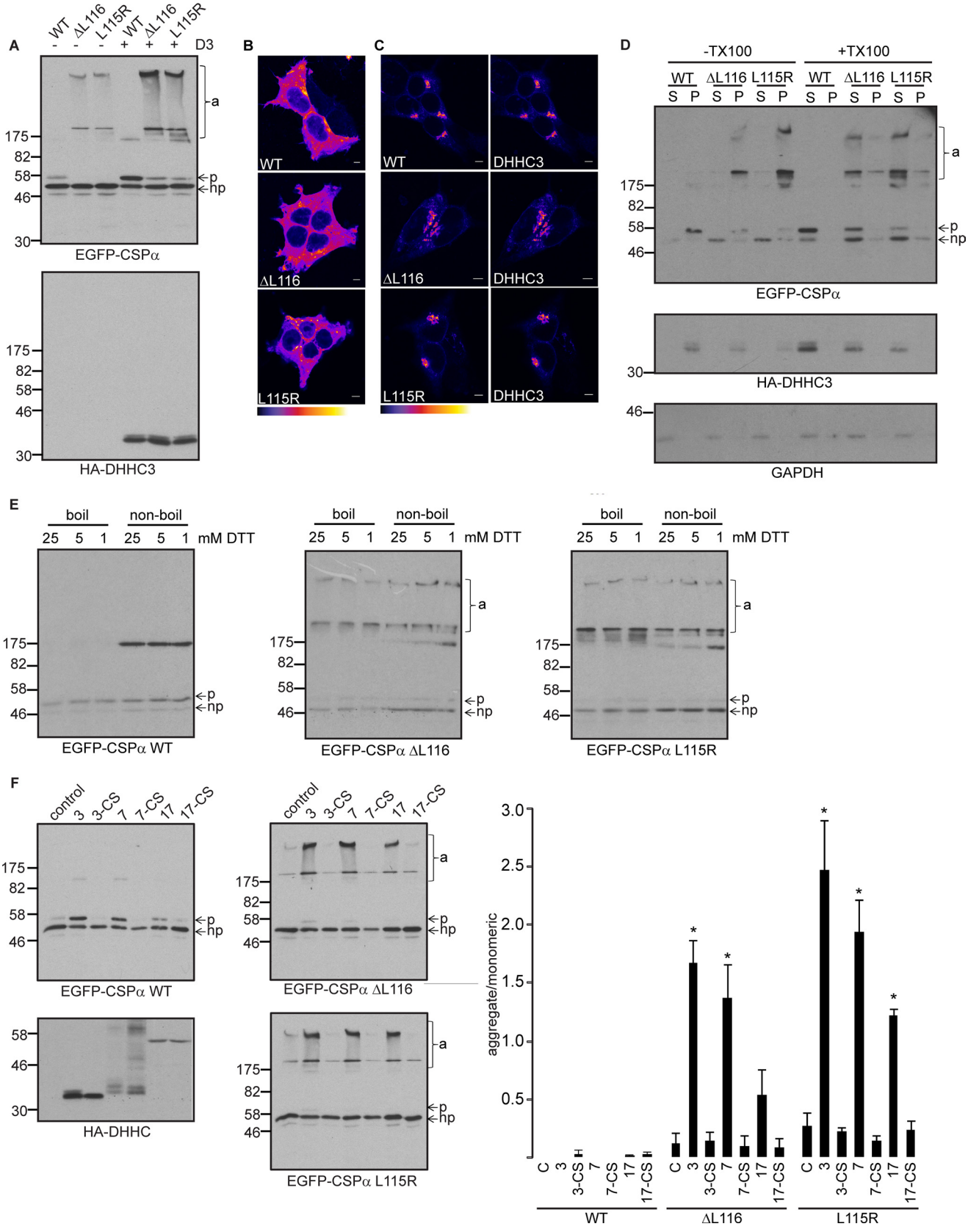

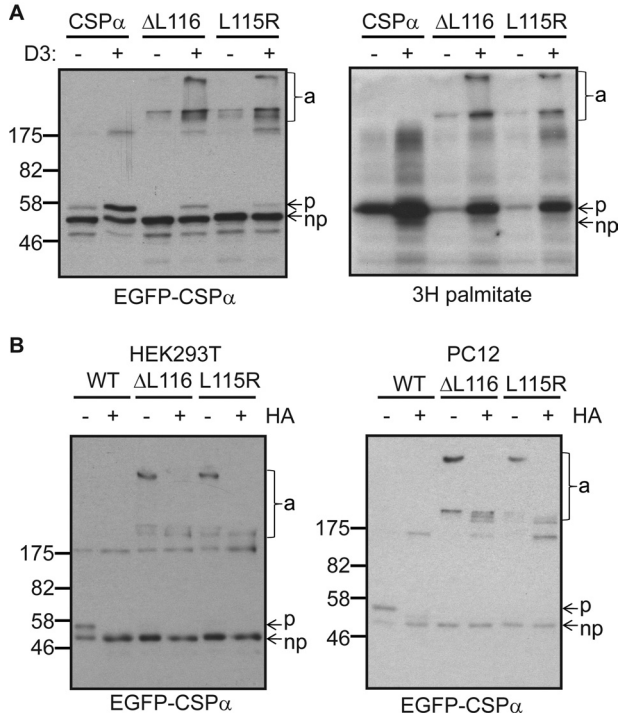

FIGURE 4. **Palmitoylation analysis of CSPα mutants.** *A*, HEK293T cells transfected with the wild-type and mutant EGFP-CSPα constructs and with (+) or without (−) HA-DHHC3 (*D3*) were labeled with 0.5 mCi/ml [^{3}H]palmitic acid for 3 h. Cells were lysed in SDS-dissociation buffer, resolved by SDS-PAGE, and transferred to nitrocellulose. Duplicate nitrocellulose membranes were either processed for detection of ^{3}H signal (*right*) or probed by immunoblotting with anti-GFP (*left*). *B*, HEK293T cells co-transfected with EGFP-CSPα constructs and DHHC3 (*left*) or PC12 cells transfected with EGFP-CSPα constructs alone (*right*) were treated with hydroxylamine (+) or Tris (−) as described under "Experimental Procedures." The samples were then resolved by SDS-PAGE and transferred to nitrocellulose for immunoblotting analysis using antibodies against EGFP. Nonpalmitoylated (*np*) and palmitoylated (*p*) monomeric CSPα are marked by *arrows*, and aggregated CSPα (*a*) is highlighted by a *bracket*. Positions of molecular mass standards are shown on the *left*.

mutants, implying that palmitoylation drives aggregate formation. To assess the palmitoylation status of the ΔL116 and L115R aggregates, HEK293T cells expressing the mutants with or without DHHC3 co-expression were labeled with [^{3}H]palmitic acid. Aggregated forms of the CSPα mutants clearly incorporated radiolabel, and this was enhanced by DHHC3 co-expression (Fig. 4*A*, *right*).

To determine whether the observed palmitoylation of the mutant proteins is important for the maintenance of aggregation, cell lysates were treated with hydroxylamine to cleave thioester linkages between cysteine residues and palmitate chains. Hydroxylamine treatment dissolved the higher molecular mass forms of L115R and ΔL116 mutants co-expressed in HEK293T cells with DHHC3 (Fig. 4*B*, *left*), confirming that their SDS-resistant aggregation requires palmitoylation. This same effect of hydroxylamine on mutant aggregates was also observed when CSPαs were expressed in PC12 cells without DHHC co-expression (Fig. 4*B*, *right*).

Aggregation of Mutant CSPα Proteins in Postmortem Samples from Patients with ANCL—The results presented thus far highlight a possible role for palmitoylation-dependent aggregation of mutant CSPα in the development of ANCL. To explore further the relevance of these findings to ANCL, brain lysates were prepared from control individuals and *DNAJC5* mutation carriers and incubated in the absence or presence of hydroxylamine to test whether palmitoylation-sensitive aggregates were present. Fig. 5 shows that high molecular mass SDS-resistant aggregates were clearly detected in samples from ANCL patients but not in control samples. Furthermore, immunoreactivity of these aggregates was greatly reduced following hydroxylamine treatment.

Co-aggregation of Mutant and Wild-type CSPα Proteins—Because mutations in CSPα cause autosomal dominant ANCL, the ΔL116 and L115R mutant proteins are toxic even in the presence of a wild-type copy of the CSPα gene. Therefore, it is possible that the mutant proteins have the capacity to interfere with the function of wild-type CSPα. We examined this by testing whether mutant CSPα proteins induced co-aggregation of wild-type CSPα. For this, HEK293T cells were transfected with myc-tagged wild-type CSPα, DHHC3, and EGFP-tagged wild-type or mutant CSPα. Fig. 6 shows that in the presence of EGFP-CSPα ΔL116 or L115R mutants, a small fraction of myc-CSPα was recruited into SDS-resistant aggregates. This was not observed following co-expression with either EGFP or EGFP-CSPα wild-type (Fig. 6). This result clearly highlights the potential of mutant CSPα proteins to interfere with the wild-type protein, offering a possible mechanism for the dominant effect of these disease-causing mutants in the development of ANCL.

DISCUSSION

The link between protein misfolding/aggregation and neurodegeneration is well established for disorders such as Alzheimer, Parkinson, and Huntington diseases (25). The results presented in this study further highlight the correlation between protein aggregation and neurodegeneration, with respect to mutant CSPα and ANCL. Perhaps the most intriguing observation in the present study is the link between aggregation of the mutant CSPα proteins and palmitoylation, highlighting the interplay between genetic mutations and post-translational modification in the induction of protein aggregation. Post-

FIGURE 3. **Active DHHC palmitoyltransferases promote aggregation of CSPα mutants.** *A*, EGFP-CSPα wild-type and ΔL116/L115R mutants were co-transfected into HEK293T cells with HA-DHHC3 (*D3*) or empty vector. Lysates were resolved by SDS-PAGE, transferred to nitrocellulose, and probed with antibodies against GFP or HA. Nonpalmitoylated (*np*) and palmitoylated (*p*) CSPα are marked by *arrows*, and aggregated (*a*) CSPα is highlighted by a *bracket*. Positions of molecular mass standards are shown on the *left*. *B* and *C*, HEK293T cells were transfected with EGFP-tagged constructs (*B*) or EGFP-tagged constructs together with HA-DHHC3 (*C*). Co-transfected cells were fixed and stained with anti-HA, followed by an anti-mouse antibody conjugated to Alexa Fluor 546. Cells were viewed using a Leica SP5 confocal microscope. *Scale bars* represent 5 μm, and the fluorescence intensity color code is shown. *D*, HEK293T cells co-expressing the indicated CSPα proteins and DHHC3 were fractionated into supernatant (*S*) and pellet (*P*) fractions, containing cytosolic and membrane proteins, respectively. The fractionation was performed in the presence and absence of 1% Triton X-100 as indicated. Equal volumes of the recovered samples were resolved by SDS-PAGE, transferred to nitrocellulose, and probed with antibodies against GFP, HA, and GAPDH. *E*, HEK293T cells co-expressing the CSPα proteins and DHHC3 were lysed in SDS-dissociation buffer containing 1, 5, or 25 mM DTT and were either heated to 100 °C (*boil*) or 37 °C (*non-boil*) for 5 min before running. *F*, cells were transfected with EGFP-CSPα and the indicated HA-DHHC proteins and analyzed as in *A*. The mean ratio of aggregated to monomeric forms of each protein under the various transfection conditions was calculated and is presented together with S.E. (*error bars*) ($n = 3$). Statistical tests were performed using a one-way ANOVA, *asterisks* denote a p value of <0.05 compared with proteins without DHHC co-expression.

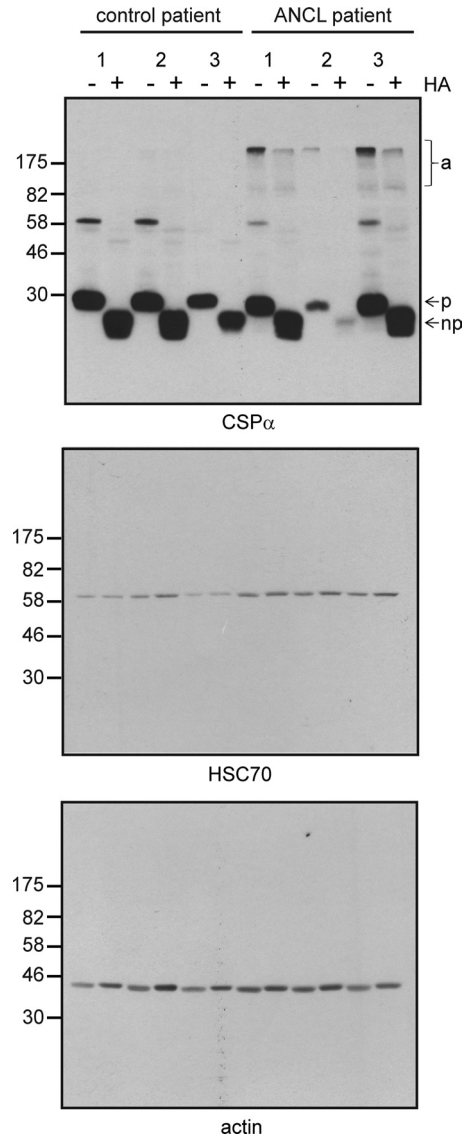

FIGURE 5. **CSPα expression and aggregation in human brain.** Cortical lysates from control and *DNAJC5* mutation carriers (three separate individuals for each) were treated with hydroxylamine (+) or Tris (−), resolved by SDS-PAGE, and transferred to nitrocellulose for immunoblotting analysis using antibodies against CSPα, HSC70, and actin. Nonpalmitoylated (*np*) and palmitoylated (*p*) monomeric CSPα are marked by *arrows*, and aggregated CSPα (*a*) is highlighted by a *bracket*. Positions of molecular mass standards are shown on the *left*.

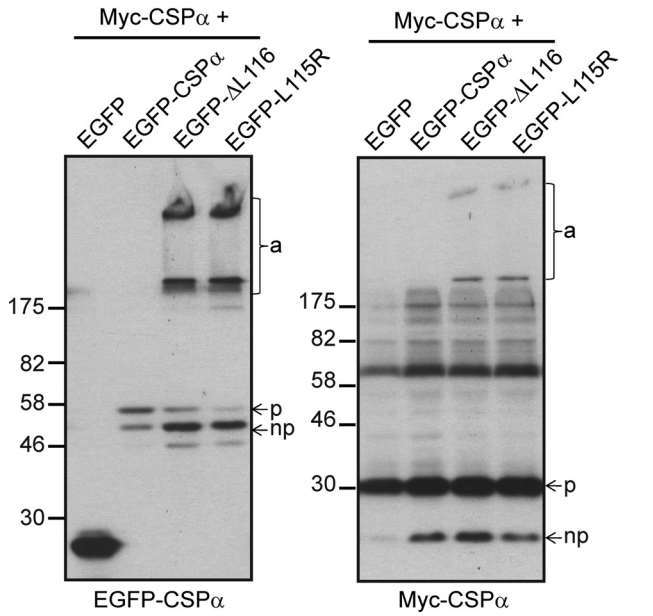

FIGURE 6. **Co-aggregation of wild-type and mutant CSPα.** HEK293T cells were transfected with HA-DHHC3, myc-tagged CSPα wild-type, and EGFP, EGFP-CSPα, EGFP-CSPα (ΔL116), or EGFP-CSPα (L115R). Cell lysates were resolved by SDS-PAGE and transferred to nitrocellulose for immunoblotting analysis using antibodies against EGFP (*left*) and myc (*right*). Nonpalmitoylated (*np*) and palmitoylated (*p*) monomeric CSPα are marked by *arrows*, and aggregated CSPα (*a*) is highlighted by a *bracket*. Positions of molecular mass standards are shown on the *left*.

translational modifications such as phosphorylation and proteolytic cleavage can modulate the aggregation of cytotoxic mutant proteins in other neurodegenerative disorders (26), and indeed blocking the palmitoylation of mutant Huntingtin increased the formation of inclusions and enhanced toxicity (27). The present study extends this link between neurodegeneration and palmitoylation and suggests that future success in counteracting ANCL in patients carrying the disease-causing CSPα mutations might be achieved by targeting the palmitoylation machinery.

It is intriguing that protein palmitoylation is implicated in both infantile and adult-onset forms of NCL, albeit by different mechanisms. A deficiency of the lysosomal thioesterase protein palmitoyl thioesterase 1 causes early onset NCL (2), and this enzyme is involved in depalmitoylation of proteins during their degradation in lysosomes (29). We speculate that the palmitoylated aggregates of CSPα mutant proteins might be less susceptible to the actions of lysosomal thioesterases, leading to a gradual accumulation of palmitoylated CSPα peptides. Thus, the difference in age of symptomatic onset between the infantile and adult-onset forms of ANCL may reflect a different rate of accumulation of nondegraded palmitoylated peptides: rapid accumulation due to a decreased cleavage of bulk palmitoylated proteins following protein palmitoyl thioesterase 1 deficiency (30) and a slower accumulation resulting from a decreased sensitivity of a single protein (mutant CSPα) to lysosomal thioesterases.

What could be the underlying cause of the observed aggregation of L115R and ΔL116 CSPα mutants? First, it is important to note that wild-type CSPα has an intrinsic tendency to self-associate (18), and indeed SDS-resistant dimers of wild-type CSPα are frequently observed in cellular samples (see Fig. 3*E*). This self-association is dramatically enhanced by the ΔL116 and L115R mutations, leading to the formation of high molecular mass SDS-resistant aggregates that are not observed with the wild-type protein. One possibility to explain these effects is that the mutations promote a restructuring of the cysteine-string domain resulting in added palmitate groups being positioned outside the hydrophobic core of the membrane bilayer. Palmitate chains of different mutant CSPα monomers might then cluster together via lipid-lipid interactions to shield the exposed palmitate chains from water. Indeed, it is possible that the CSPα monomers within the aggregates are not fully palmitoylated. This is implied by the lower [^{3}H]palmitate signal from aggregates compared with monomeric protein; for example, for

the data presented in Fig. 4*A* the ^{3}H signal for the ΔL116 and L115R high molecular mass aggregates was 5.8- and 12.5-fold, respectively, less than that from the corresponding monomers when normalized to protein levels. This difference might suggest that the aggregates contain partially palmitoylated mutant monomers or a mixture of palmitoylated and nonpalmitoylated monomers. At present we remain cautious in our interpretation of the different ^{3}H signals from monomeric and aggregated protein. In particular, it is not clear whether palmitate turnover on the monomers and aggregates occurs with similar kinetics or even whether the aggregation of mutant CSPα somehow reduces the ^{3}H signal from associated palmitate chains. Disrupting the mutant CSPα aggregates into their constituent monomers, without perturbing palmitoylation, would provide a clearer indication of the palmitoylation status of individual monomers within the aggregates; this is an area of investigation that we are currently pursuing. Another possibility to explain the palmitoylation-dependent aggregation is that the mutant proteins are intrinsically more prone to self-associate (in their nonpalmitoylated state). In this case, palmitoylation-induced membrane binding might simply concentrate the mutant proteins on cellular membranes facilitating aggregate formation in a manner that does not directly involve palmitate chains. Although this model is supported by the observation that bacterially expressed recombinant CSPα self-associates via a region containing the cysteine-string domain (18), this does not readily fit with our data showing that the high molecular mass mutant aggregates are disassembled by hydroxylamine treatment.

Another point of note is that complete knock-out of CSPα in mice causes neurodegeneration (11). Thus, it is possible that disease occurs in humans carrying the L115R/ΔL116 mutations as a result of reduced levels of wild-type CSPα. However, the finding that CSPα heterozygous knock-out mice have no overt neurodegenerative phenotype might argue against this possibility (11). Nevertheless, mutant forms of CSPα could exhibit a toxic gain-of-function effect through interfering with the function or trafficking of wild-type CSPα. Indeed, it was suggested that there was a loss of immunofluorescence signal and synaptic targeting of CSPα in cerebral and cerebellar cortex samples from a L115R mutation carrier (6). We detected the recruitment of small amounts of myc-tagged wild-type CSPα protein into EGFP-tagged mutant aggregates (Fig. 6), and thus aggregates containing both mutant and wild-type CSPα in the brains of ANCL patients are a possibility. Co-aggregation of wild-type and mutant CSPα may perturb synaptic targeting, leading to destabilization of key synaptic proteins such as the SNARE protein SNAP25 (31). The mutant aggregates might also cause cellular toxicity by recruiting and sequestering other key cellular proteins (28).

At present we are not certain why Nosková *et al.* (6) failed to detect a major loss of palmitoylation of mutant EGFP-CSPα constructs in CAD5 cells. However, we note that the authors did not confirm the identity of immunoreactive bands that were proposed to represent palmitoylated and nonpalmitoylated CSPα (for example, by using hydroxylamine treatment). Full-length immunoblots were also not presented in this study, preventing an assessment of protein aggregation, although hydroxylamine treatment of brain samples from an affected individual that lacked CSPα immunoreactivity led to the appearance of an immunoreactive band that may represent a dimeric form of CSPα (6).

In summary, the results presented further highlight the relationship between protein aggregation and neurodegeneration, while revealing a novel role for palmitoylation in driving aggregation of disease-causing mutants.

Acknowledgment—We thank Masaki Fukata for providing the HA-tagged DHHC constructs.

REFERENCES

1. Jalanko, A., and Braulke, T. (2009) Neuronal ceroid lipofuscinoses. *Biochim. Biophys. Acta* **1793,** 697–709
2. Vesa, J., Hellsten, E., Verkruyse, L. A., Camp, L. A., Rapola, J., Santavuori, P., Hofmann, S. L., and Peltonen, L. (1995) Mutations in the palmitoyl protein thioesterase gene causing infantile neuronal ceroid lipofuscinosis. *Nature* **376,** 584–587
3. Camp, L. A., and Hofmann, S. L. (1993) Purification and properties of a palmitoyl-protein thioesterase that cleaves palmitate from H-Ras. *J. Biol. Chem.* **268,** 22566–22574
4. Shacka, J. J. (2012) Mouse models of neuronal ceroid lipofuscinoses: useful pre-clinical tools to delineate disease pathophysiology and validate therapeutics. *Brain Res. Bull.* **88,** 43–57
5. Velinov, M., Dolzhanskaya, N., Gonzalez, M., Powell, E., Konidari, I., Hulme, W., Staropoli, J. F., Xin, W., Wen, G. Y., Barone, R., Coppel, S. H., Sims, K., Brown, W. T., and Züchner, S. (2012) Mutations in the gene *DNAJC5* cause autosomal dominant Kufs disease in a proportion of cases: study of the Parry family and 8 other families. *PLoS ONE* **7,** e29729
6. Nosková, L., Stránecký, V., Hartmannová, H., Přistoupilová, A., Barešová, V., Ivánek, R., Hůlková, H., Jahnová, H., van der Zee, J., Staropoli, J. F., Sims, K. B., Tyynelä, J., Van Broeckhoven, C., Nijssen, P. C. , Mole, S. E., Elleder, M., and Kmoch, S. (2011) Mutations in *DNAJC5*, encoding cysteine-string protein α, cause autosomal-dominant adult-onset neuronal ceroid lipofuscinosis. *Am. J. Hum. Genet.* **89,** 241–252
7. Benitez, B. A., Alvarado, D., Cai, Y., Mayo, K., Chakraverty, S., Norton, J., Morris, J. C., Sands, M. S., Goate, A., and Cruchaga, C. (2011) Exome-sequencing confirms *DNAJC5* mutations as cause of adult neuronal ceroid-lipofuscinosis. *PLoS ONE* **6,** e26741
8. Chamberlain, L. H., and Burgoyne, R. D. (1998) Cysteine string protein functions directly in regulated exocytosis. *Mol. Biol. Cell* **9,** 2259–2267
9. Zhang, H., Kelley, W. L., Chamberlain, L. H., Burgoyne, R. D., Wollheim, C. B., and Lang, J. (1998) Cysteine-string proteins regulate exocytosis of insulin independent from transmembrane ion fluxes. *FEBS Lett.* **437,** 267–272
10. Chamberlain, L. H., and Burgoyne, R. D. (2000) Cysteine-string protein: the chaperone at the synapse. *J. Neurochem.* **74,** 1781–1789
11. Fernández-Chacón, R., Wölfel, M., Nishimune, H., Tabares, L., Schmitz, F., Castellano-Muñoz, M., Rosenmund, C., Montesinos, M. L., Sanes, J. R., Schneggenburger, R., and Südhof, T. C. (2004) The synaptic vesicle protein CSPα prevents presynaptic degeneration. *Neuron* **42,** 237–251
12. Sharma, M., Burré, J., Bronk, P., Zhang, Y., Xu, W., and Südhof, T. C. (2012) CSPα knockout causes neurodegeneration by impairing SNAP-25 function. *EMBO J.* **31,** 829–841
13. Jahn, R., and Scheller, R. H. (2006) SNAREs: engines for membrane fusion. *Nat. Rev. Mol. Cell. Biol.* **7,** 631–643
14. Rozas, J. L., Gómez-Sánchez, L., Mircheski, J., Linares-Clemente, P., Nieto-González, J. L., Vázquez, M. E., Luján, R., and Fernández-Chacón, R. (2012) Motorneurons require cysteine string protein-α to maintain the readily releasable vesicular pool and synaptic vesicle recycling. *Neuron* **74,** 151–165
15. Zhang, Y. Q., Henderson, M. X., Colangelo, C. M., Ginsberg, S. D., Bruce, C., Wu, T., and Chandra, S. S. (2012) Identification of CSPα clients reveals a role in dynamin 1 regulation. *Neuron* **74,** 136–150

16. Greaves, J., and Chamberlain, L. H. (2006) Dual role of the cysteine-string domain in membrane binding and palmitoylation-dependent sorting of the molecular chaperone cysteine-string protein. *Mol. Biol. Cell* **17,** 4748–4759
17. Greaves, J., Salaun, C., Fukata, Y., Fukata, M., and Chamberlain, L. H. (2008) Palmitoylation and membrane interactions of the neuroprotective chaperone cysteine-string protein. *J. Biol. Chem.* **283,** 25014–25026
18. Swayne, L. A., Blattler, C., Kay, J. G., and Braun, J. E. (2003) Oligomerization characteristics of cysteine string protein. *Biochem. Biophys. Res. Comm.* **300,** 921–926
19. Fukata, M., Fukata, Y., Adesnik, H., Nicoll, R. A., and Bredt, D. S. (2004) Identification of PSD-95 palmitoylating enzymes. *Neuron* **44,** 987–996
20. Millar, T., Walker, R., Arango, J. C., Ironside, J. W., Harrison, D. J., MacIntyre, D. J., Blackwood, D., Smith, C., and Bell, J. E. (2007) Tissue and organ donation for research in forensic pathology: the MRC Sudden Death Brain and Tissue Bank. *J. Pathol.* **213,** 369–375
21. Grefen, C., Obrdlik, P., and Harter, K. (2009) The determination of protein-protein interactions by the mating-based split-ubiquitin system (mbSUS). *Methods Mol. Biol.* **479,** 217–233
22. Gorleku, O. A., Barns, A. M., Prescott, G. R., Greaves, J., and Chamberlain, L. H. (2011) Endoplasmic reticulum localization of DHHC palmitoyltransferases mediated by lysine-based sorting signals. *J. Biol. Chem.* **286,** 39573–39584
23. Greaves, J., and Chamberlain, L. H. (2011) DHHC palmitoyl transferases: substrate interactions and (patho)physiology. *Trends Biochem. Sci.* **36,** 245–253
24. Ohyama, T., Verstreken, P., Ly, C. V., Rosenmund, T., Rajan, A., Tien, A. C., Haueter, C., Schulze, K. L., and Bellen, H. J. (2007) Huntingtin-interacting protein 14, a palmitoyl transferase required for exocytosis and targeting of CSP to synaptic vesicles. *J. Cell Biol.* **179,** 1481–1496
25. Polymenidou, M., and Cleveland, D. W. (2011) The seeds of neurodegeneration: prion-like spreading in ALS. *Cell* **147,** 498–508
26. Humbert, S., Bryson, E. A., Cordelières, F. P., Connors, N. C., Datta, S. R., Finkbeiner, S., Greenberg, M. E., and Saudou, F. (2002) The IGF-1/Akt pathway is neuroprotective in Huntington's disease and involves Huntingtin phosphorylation by Akt. *Dev. Cell* **2,** 831–837
27. Yanai, A., Huang, K., Kang, R., Singaraja, R. R., Arstikaitis, P., Gan, L., Orban, P. C., Mullard, A., Cowan, C. M., Raymond, L. A., Drisdel, R. C., Green, W. N., Ravikumar, B., Rubinsztein, D. C., El-Husseini, A., and Hayden, M. R. (2006) Palmitoylation of huntingtin by HIP14 is essential for its trafficking and function. *Nat. Neurosci.* **9,** 824–831
28. Olzscha, H., Schermann, S. M., Woerner, A. C., Pinkert, S., Hecht, M. H., Tartaglia, G. G., Vendruscolo, M., Hayer-Hartl, M., Hartl, F. U., and Vabulas, R. M. (2011) Amyloid-like aggregates sequester numerous metastable proteins with essential cellular functions. *Cell* **144,** 67–78
29. Verkruyse, L. A., and Hofmann, S. L. (1996) Lysosomal targeting of palmitoyl-protein thioesterase. *J. Biol. Chem.* **271,** 15831–15836
30. Lu, J. Y., Verkruyse, L. A., and Hofmann, S. L. (1996) Lipid thioesters derived from acylated proteins accumulate in infantile neuronal ceroid lipofuscinosis: correction of the defect in lymphoblasts by recombinant palmitoyl-protein thioesterase. *Proc. Natl. Acad. Sci. U.S.A.* **93,** 10046–10050
31. Sharma, M., Burré, J., and Südhof, T. C. (2011) CSPα promotes SNARE-complex assembly by chaperoning SNAP-25 during synaptic activity. *Nat. Cell Biol.* **13,** 30–39